Comparison of Six Robustness Tests Evaluating Missile Autopilot Robustness to Uncertain Aerodynamics

Kevin A. Wise*

McDonnell Douglas Missile Systems Company, St. Louis, Missouri 63166

The robustness of an acceleration command missile autopilot to uncertain aerodynamic parameters is determined using six robustness tests: 1) small gain theorem, 2) structured singular value, 3) stability hypersphere— polynomial, 4) stability hypersphere—Lyapunov, 5) Kharitonov's theorem, and 6) multiloop stability margin. Parameter variation tolerances were also determined by a Monte Carlo eigenanalysis and are compared with the theoretical predictions.

Introduction

A MISSILE flight control system must guarantee stability and performance in the face of large aerodynamic uncertainties and disturbances. This requires the feedback controller to maintain system stability and loop performance for all possible variations in the plant behavior. Determination of the degree of robustness to these aerodynamic uncertainties is the focus of this paper.

Missile autopilots are designed using linear models of the nonlinear equations of motion and aerodynamic forces and moments. The aerodynamic parameters contained in this model are derived from wind-tunnel measurements on a scaled missile model. Aerodynamic stability derivatives model the force and moments acting on the missile body and fins. By quantifying missile autopilot sensitivity to variations in these aerodynamic parameters, the missile flight control system can be designed with much greater performance.

The robustness tests evaluated here were used to determine bounds on variations in the aerodynamic parameters. They are applicable only to linear time-invariant analysis models. These robustness tests were applied to a bank-to-turn missile longitudinal (pitch) flight control system.

The robustness tests examined are categorized as follows: 1) singular value robustness tests—small gain theorem, and structured singular value μ-test; 2) stability hypersphere radius calculation—polynomial model and Lyapunov (state space); 3) Kharitonov's theorem—polynomial model; and 4) real stability margin calculation—deGaston-Safonov algorithm.

The singular value robustness tests include the small gain theorem (SGT) and the structured singular value (SSV) μ-test of Doyle[1] and Doyle et al.[2] Wise[3] used these singular-value-based tests to determine input and output loop break point stability margins, and in analyzing missile autopilot robustness to neglected/mismodeled actuator dynamics and neglected bending dynamics (all were complex uncertainties). In this paper, these tests are used to analyze real parameter variations.

The stability hypersphere radius is the two norm of the parameter perturbation vector. These robustness tests were taken from Biernacki et al.[4] and Bhattacharyya.[5] A detailed presentation of these robustness tests applied to a missile autopilot is made in Wise[6] and is summarized here for comparison.

A myriad of papers have recently been published that utilize Kharitonov's theorem[7] and variants thereof. Kharitonov's

theorem analyzes the robustness question by examining the Hurwitz properties of a family of polynomials whose coefficients are based on the system's characteristic equation and uncertain parameters. Barmish and DeMarco[8] present an excellent literature review on these polynomial methods. The variant of Kharitonov's theorem used in this paper is taken from Argoun.[9]

DeGaston and Safonov[10] recently published a parameter space method for exactly determining control system robustness to real parameter variations. This approach was then modified by Sideris and Pena[11] to reduce the computational burden. The deGaston-Safonov algorithm is used here to analyze missile autopilot robustness to real parameter variations.

Autopilot and Missile Dynamics

The longitudinal flight control system for a bank-to-turn missile is shown in Fig. 1. Each controller block contains proportional-plus-integral control elements. In Fig. 1, the transfer function matrix $K(s)$ describes only controller dynamics. The nominal rigid-body longitudinal dynamics, containing uncertain aerodynamic parameters, is represented by $G(s)$.

The autopilot $K(s)$ is described by the following state-space quadruple

$$A_c = \begin{bmatrix} 0 & 0 \\ K_q a_q & 0 \end{bmatrix}, \qquad B_c = \begin{bmatrix} K_a a_z & 0 \\ K_a K_q a_q & K_q a_q \end{bmatrix}$$

$$C_C = [K_q \quad 1], \qquad D_c = [K_a K_q \quad K_q] \qquad (1)$$

where $K(s) = C_c(sI - A_c)^{-1}B_c + D_c$. The inputs to the autopilot $K(s)$ are commanded acceleration minus measured acceleration and the negative of the pitch rate q. The output of the autopilot is fin deflection command δ_c (rad). This autopilot design is taken from Wise.[12] The autopilot feedback gains are $K_a = -0.0015$, $K_q = -0.32$, $a_z = 2.0$, and $a_q = 6.0$.

The states modeled in the open-loop rigid-body airframe model are α, q, δ, and $\dot{\delta}$ (angle-of-attack, pitch rate, fin deflection, and fin rate, respectively). In state-space form, the
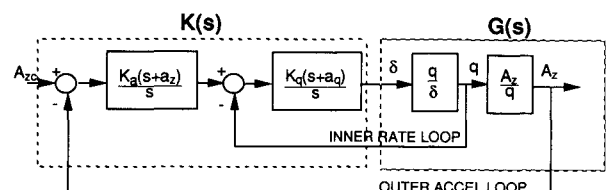
*Staff Specialist, Advanced Guidance, Navigation, and Control, Mail Code 3064025, P.O. Box 516. Senior Member AIAA.

Fig. 1 Longitudinal autopilot.

airframe dynamics are represented by the following state-space triple (A, B, C):

$$A = \begin{bmatrix} Z_\alpha & 1 & Z_\delta & 0 \\ M_\alpha & 0 & M_\delta & 0 \\ 0 & 0 & 0 & 1 \\ 0 & 0 & -\omega^2 & -2\zeta\omega \end{bmatrix}, \qquad B = \begin{bmatrix} 0 \\ 0 \\ 0 \\ \omega^2 \end{bmatrix}$$

$$C = \begin{bmatrix} VZ_\alpha & 0 & VZ_\delta & 0 \\ 0 & 1 & 0 & 0 \end{bmatrix} \qquad (2)$$

where $G(s) = C(sI - A)^{-1}B$. The plant outputs are normal acceleration A_z (ft/s^2) and pitch rate q (rad/s).

These aerodynamics have been linearized about a trim angle of attack of 16 deg, Mach 0.8, and altitude of 4000 ft. The airframe is open loop unstable. The following parameters are the nominal values of the dimensional aerodynamic stability derivatives used in this analysis:

$$Z_\alpha = -1.3046 \quad 1/s$$

$$Z_\delta = -0.2142 \quad 1/s$$

$$M_\alpha = 47.7109 \quad 1/s^2$$

$$M_\delta = -104.8346 \quad 1/s^2 \qquad (3)$$

The remaining system parameters, which are assumed known, are missile velocity $V = 886.78$ ft/s, actuator damping $\zeta = 0.6$, and actuator natural frequency $\omega = 113.0$ rad/s.

The transfer function description of the open-loop system is

$$G(s) = \begin{bmatrix} \dfrac{\omega^2 V(Z_\delta s^2 + Z_\alpha M_\delta - Z_\delta M_\alpha)}{(s^2 - Z_\alpha s - M_\alpha)(s^2 + 2\zeta\omega s + \omega^2)} \\ \dfrac{\omega^2(M_\delta s + M_\alpha Z_\delta - M_\delta Z_\alpha)}{(s^2 - Z_\alpha s - M_\alpha)(s^2 + 2\zeta\omega s + \omega^2)} \end{bmatrix} \qquad (4)$$

Note that the acceleration transfer function contains a right half-plane zero.

The autopilot design $K(s)$ stabilizes the nominal plant model $G(s)$ using output feedback, as shown in Fig. 1. The problem is to determine the perturbation bounds on the imprecisely known, dimensional, aerodynamic stability derivatives such that the closed-loop system remains stable.

Robustness Analysis Model

A state-space analysis model is formed by isolating the real parameter uncertainties and transforming the missile flight control system into the block diagonal perturbation (BDP) structure. The BDP structure of Fig. 2, with $\Delta = 0$, is a description of the nominal closed-loop system. Morton[14] has developed a systematic procedure for computing the transfer function matrix $M(s)$. Using the rigid-body open-loop airframe model (A, B, C) and autopilot model (A_c, B_c, C_c, D_c), the closed-loop system is

$$\begin{bmatrix} \dot{x} \\ \dot{x}_c \end{bmatrix} = \begin{bmatrix} A - BD_cC & BC_c \\ -B_cC & A_c \end{bmatrix}\begin{bmatrix} x \\ x_c \end{bmatrix}$$

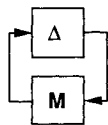$$+ \begin{bmatrix} BD_c \\ B_c \end{bmatrix}r = A_{cl}x + Fr \qquad (5)$$

Fig. 2   Block diagonal analysis model.

The uncertain aeroparameters in A_{cl} are

$$p = [Z_\alpha \ Z_\delta \ M_\alpha \ M_\delta]^T \qquad (6)$$

The uncertain parameters in Eq. (6) are modeled using $p = p_0 + \Delta p$. Let $\Delta p_i = p_{0i}\delta_i$, with $p_i = p_{0i}(1 + \delta_i)$. The closed-loop matrix is modeled as

$$A_{cl} = A_0 + E_1\delta Z_\alpha + E_2\delta Z_\delta + E_3\delta M_\alpha + E_4\delta M_\delta \qquad (7)$$

where δZ_α, δZ_δ, δM_α, and δM_δ are variations in the aerodynamic stability derivatives. The nominal closed-loop matrix A_0 is stable and is given by Eq. (5) using the nominal parameter values. Let δ_i, $i = 1, 4$, describe each of the variations in Eq. (7). The uncertainties enter the closed-loop system through the matrices E_i. The matrices E_i in Eq. (7) are

$$E_1 = \begin{bmatrix} Z_\alpha & 0 & 0 & 0 & 0 & 0 \\ 0 & 0 & 0 & 0 & 0 & 0 \\ 0 & 0 & 0 & 0 & 0 & 0 \\ -\omega^2 K_a K_q VZ_\alpha & 0 & 0 & 0 & 0 & 0 \\ -K_a a_z VZ_\alpha & 0 & 0 & 0 & 0 & 0 \\ -K_a K_q a_q VZ_\alpha & 0 & 0 & 0 & 0 & 0 \end{bmatrix}$$

$$E_2 = \begin{bmatrix} 0 & 0 & Z_\delta & 0 & 0 & 0 \\ 0 & 0 & 0 & 0 & 0 & 0 \\ 0 & 0 & 0 & 0 & 0 & 0 \\ 0 & 0 & -\omega^2 K_a K_q VZ_\delta & 0 & 0 & 0 \\ 0 & 0 & -K_a a_z VZ_\delta & 0 & 0 & 0 \\ 0 & 0 & -K_a K_q a_q VZ_\delta & 0 & 0 & 0 \end{bmatrix}$$

$$E_3 = \begin{bmatrix} 0 & 0 & 0 & 0 & 0 & 0 \\ M_\alpha & 0 & 0 & 0 & 0 & 0 \\ 0 & 0 & 0 & 0 & 0 & 0 \\ 0 & 0 & 0 & 0 & 0 & 0 \\ 0 & 0 & 0 & 0 & 0 & 0 \\ 0 & 0 & 0 & 0 & 0 & 0 \end{bmatrix}$$

$$E_4 = \begin{bmatrix} 0 & 0 & 0 & 0 & 0 & 0 \\ 0 & 0 & M_\delta & 0 & 0 & 0 \\ 0 & 0 & 0 & 0 & 0 & 0 \\ 0 & 0 & 0 & 0 & 0 & 0 \\ 0 & 0 & 0 & 0 & 0 & 0 \\ 0 & 0 & 0 & 0 & 0 & 0 \end{bmatrix} \qquad (8)$$

When using state-space models to analyze parameter uncertainties, the rank of the matrix E_i is used to describe the perturbation. The four parameters here are all rank 1 perturbations (in Wise,[3] a rank 2 perturbation caused by variations in dynamic pressure was analyzed). Equation (8) is rewritten as

$$A_{cl} = A_0 + \sum_{i=1}^{n} E_i\delta_i \qquad (9)$$

In Eq. (9), the matrices E_i are the structural definitions for each of the parameter perturbations δ_i. Each multiplicative uncertainty δ_i represents a percentage variation in a parameter. Using this model, decompose each $n \times n$ matrix E_i using a singular value decomposition. Thus,

$$E_i = U\Sigma V^* \qquad (10)$$

The matrix Σ will have k_i nonzero singular values, where k_i is equal to the rank of the matrix E_i. The rank $(E_i) = k_i$ denotes the rank of the perturbation δ_i. [If rank $(E_i) = 2$ then δ_i is a rank 2 perturbation.] The matrix Σ will have k_i nonzero singular values with the remaining $n - k_i$ singular values equal to zero. Discard the zero singular values and make Σ a $k_i \times$

k_i diagonal matrix containing only the nonzero singular values. We can write Eq. (10) with this new Σ as

$$E_i = \beta_i \alpha_i \qquad (11)$$

where $\beta_i = U(\Sigma)^{\frac{1}{2}}$ and $\alpha_i = (\Sigma)^{\frac{1}{2}}V^*$. The matrices β_i and α_i in Eq. (11) depend only on the magnitude of the ith nominal parameter. By using the decomposition described in Eq. (11), we can replace $E_i\delta_i$ in Eq. (9) with $\beta_i\alpha_i\delta_i$. By using this model, we can separate out the parameter variations δ_i, form $\Delta = \text{diag}[\delta_i]$, and create the nominally stable $M(s) = C_m(sI - A_m)^{-1}B_m$. The state-space triple (A_m, B_m, C_m) for $M(s)$ is formed as follows.

Consider rank 1 perturbations only. β_i is $n \times 1$ and α_i is $1 \times n$. Thus, Eq. (9) is

$$A_{cl} = A_0 + \sum_{i=1}^{n} \beta_i\delta_i\alpha_i \qquad (12)$$

with $-1 < \delta_i < 1$. Write the closed-loop system as

$$\dot{x} = A_0 x + \sum_{i=1}^{n} \beta_i u_i \qquad (13)$$

where the u_i are input variables. Let the output y be defined as

$$y = \sum_{i=1}^{n} \alpha_i x = \begin{bmatrix} \alpha_1 \\ \vdots \\ \alpha_n \end{bmatrix} x \qquad (14)$$

Then, if $u_i = \delta_i y_i$, we can close the loop with

$$u_i = \delta_i y_i = \delta_i \alpha_i x \qquad (15)$$

Substituting Eq. (15) into Eq. (13) yields

$$\dot{x} = (A_0 + \sum_{i=1}^{n} E_i\delta_i)x = A_{cl}x \qquad (16)$$

which is the closed-loop system model. We can write a state-space triple (A_m, B_m, C_m) for this system as

$$A_m = A_0, \qquad B_m = [\beta_1 \cdots \beta_n], \qquad C_m = \begin{bmatrix} \alpha_1 \\ \vdots \\ \alpha_n \end{bmatrix} \qquad (17)$$

This triple describes the M block in Fig. 2.

Missile Autopilot Robustness

This section presents results from six robustness tests computing bounds on the aerodynamic stability derivatives.

Singular Value Robustness Tests

The small gain theorem and the structured singular value μ-test can both be used to bound the real parameter variations. These tests assume the uncertainties modeled in Δ are complex valued. When applied to problems analyzing real parameter uncertainties, they are conservative.

Both the SGT and SSV tests use the same BDP analysis model developed in the previous section. Using the BDP structure, stability of the uncertain system is equivalent to

$$\det[I + M\Delta] \neq 0 \qquad (18)$$

By definition, the maximum and minimum singular values of the matrix A are

$$\bar{\sigma}[A] = \max_{x \neq 0} \frac{\|Ax\|_2}{\|x\|_2} = \|A\|_2 \qquad (19a)$$

$$\underline{\sigma}[A] = \min_{x \neq 0} \frac{\|Ax\|_2}{\|x\|_2} = \frac{1}{\|A^{-1}\|_2} \qquad \text{if } A^{-1} \text{ exists} \qquad (19b)$$

The minimum singular value $\underline{\sigma}[A]$ measures the near singularity of A.

The object of the singular value robustness tests is to bound the size of Δ, viewed through a matrix norm, such that Eq. (18) is satisfied. If the $\det[I + M\Delta] = 0$, then the matrix $I + M\Delta$ is singular. Let $I + M\Delta = A + B$. If $A + B$ is singular, then $A + B$ is rank deficient. Since $A + B$ is rank deficient, there exists an $x \neq 0$ such that $\|x\|_2 = 1$ and $(A + B)x = 0$ [x is in the Ker$(A + B)$]. Using $(A + B)x = 0$, we obtain $Ax + Bx = 0, Ax = -Bx$, and $\|Ax\|_2 = \|Bx\|_2$. Equations (19) combined with this $\|x\|_2$ yields

$$\underline{\sigma}[A] \leq \|Ax\|_2 = \|Bx\|_2 \leq \|B\|_2 = \bar{\sigma}[B] \qquad (20)$$

This above inequality says that $\underline{\sigma}[A] < \bar{\sigma}[B]$ for $A + B$ to be singular. If $\underline{\sigma}[A] > \bar{\sigma}[B]$, then $A + B$ is nonsingular. Substituting $A = I$ and $B = M\Delta$, we obtain

$$\underline{\sigma}[I] = 1 > \bar{\sigma}[M\Delta] \qquad (21)$$

Using $\bar{\sigma}[M\Delta] < \bar{\sigma}[M]\bar{\sigma}[\Delta]$, we obtain the SGT

$$\bar{\sigma}[\Delta] < 1/\bar{\sigma}[M] \qquad (22)$$

This inequality is a sufficient test for stability. If it is violated, the system may still be stable. In order to bound the magnitude of the real parameter variations modeled in Δ, we use the minimum of the $1/\bar{\sigma}[M]$ frequency response, and use this bound at all frequencies. The conservatism in this bound is due to the two-norm measure $\|M\|_2$. This bound on Δ assumes that Δ is a full matrix, when in fact it is diagonal. This is a conservative bound on Δ produced by the SGT.

The SSV analysis utilizes a block diagonal structure for Δ in Eq. (22) to develop a less conservative analysis. Using this restriction for Δ, the size of Δ is limited through the restriction:

$$\bar{\sigma}[\Delta] < 1/\mu \qquad (23)$$

The problem is to find the smallest μ such that for a block diagonal Δ the system remains stable. The SGT would ignore the structure of Δ and would result in $\mu = \bar{\sigma}[M]$, which is a worse case scenario (this would assume Δ to be a full single-block matrix, which would be conservative if Δ was actually block diagonal). Since the off-diagonal terms in Δ are restricted to be zero by the block diagonal restriction, $\mu < \bar{\sigma}[M]$ with a strong inequality for diagonal Δ. A detailed derivation of the SSV μ can be found in Doyle.[1]

The SSV μ is computed by bounding μ through the following optimization:

$$\max_{W}|\lambda_{max}(WM)| < \mu < \inf_{D}\bar{\sigma}[DMD^{-1}]$$

The SSV μ software used in this paper computes only the upper bound on μ using the D-matrix optimization. Since the M matrix is frequency dependent, the D-matrix optimization is swept over a range of frequencies. The minimum of the $1/\mu$ frequency response is used to bound $\bar{\sigma}[\Delta]$. Directional information from the SSV lower bound would identify the parameter variation that causes instability (see Ref. 16). This information is not available using our analysis software.

Figure 3 shows the results of an SSV μ-test using the $M\Delta$ robustness analysis model. The $1/\mu$ frequency response bounds $\bar{\sigma}[\Delta]$. Since Δ is a diagonal matrix, this bounds the absolute value of each δ_i. Figure 3 also displays the $1/\bar{\sigma}[M]$ frequency response. Using $1/\bar{\sigma}[M]$ to bound $\bar{\sigma}[\Delta]$ is an application of the SGT. The minimum of these frequency responses is used to bound the parameter variations. Figure 3 shows that the SSV μ-test produces a less conservative robustness prediction

than the SGT. The SSV μ-test computes a 49% variation bound on the δ_i. The SGT produces a 13.8% variation bound.

Stability Hypersphere Radius Calculation

Three stability hypersphere robustness tests are used to predict bounds on real the parameter variations. These robustness tests were published by Biernacki et al.[4] and Bhattacharyya.[5] Two of these tests use polynomial models of the airframe/autopilot control system. The third test (Lyapunov approach) uses a state-space model.

Polynomial-Based Approach

For the hypersphere tests, the uncertain parameters are arranged into a vector $p = p_0 + \Delta p$, where p_0 is a nominal design condition and Δp denotes the parameter variations. The stability hypersphere radius, denoted $\rho(p_0)$, is the two norm of the vector Δp, and is shown in Fig. 4a for a two-dimensional parameter space. The circle centered at the stable nominal design point is tangent to the parameter region in which the closed-loop system would be unstable. The radius of this circle is the stability hypersphere radius. The $\rho(p_0)$ shown in Fig. 4a predicts a conservative measure for parameter p_2. This conservatism is reduced by computing the stability hyperellipsoid shown in Fig. 4b. The stability hyperellipsoid is computed by scaling the parameters to lie in a unit-norm bounded sphere, computing the stability hypersphere for the scaled system and then scaling back to the original parameter space.

The polynomial-based stability hypersphere radius calculations are obtained by mapping the uncertain parameter vec-

Fig. 3   Singular value robustness tests.

Fig. 4   Stability hypersphere and hyperellipsoid.

tor p into the space of closed-loop characteristic polynomials (CLCP) $\delta(s)$ and determining how large Δp can be such that the CLCPs remain Hurwitz. The polynomial coefficients of $\delta(s) = \delta_n s^n + \cdots + \delta_1 s + \delta_0$ are arranged into the closed-loop characteristic vector (CLCV) $\delta = [\delta_n \cdots \delta_1 \delta_0]^T$. The controller maps the parameter vector p into δ through the linear mapping $Xp = \delta$. The matrix X contains polynomial coefficients from the controller transfer functions. The parameter vector p contains the nonzero numerator and denominator polynomial coefficients from the missile airframe transfer function model.

The CLCV δ fails to be Hurwitz if $\delta_n \to 0$, $\delta_0 \to 0$, or if any of the interior roots cross the $j\omega$ axis. If $\delta_0 \to 0$, then a pole at $s = 0$ is formed, and the system is no longer asymptotically stable. If $\delta_n \to 0$, then a pole at $s = \infty$ is formed. Denote Δ_0 as the set of CLCVs with $\delta_0 = 0$, Δ_n as the set of CLCV with $\delta_n = 0$, and Δ_ω as the set of CLCV's with two roots on the $j\omega$ axis. The sets Δ_0, Δ_n, and Δ_ω contain parameter vectors that cause the closed-loop system to be unstable.

The stability hypersphere robustness tests measure the Euclidean distance between the nominal parameter vector p_0 and the parameter vectors contained in the sets Δ_0, Δ_n, and Δ_ω. To determine what parameters are contained in these sets, define the inverse images of these sets, with respect to the controller map X, in the parameter space of p. Define:

$$\Pi_0 = X^{-1}(\Delta_0) = \{p | p \in R^k, Xp \in \Delta_0\}$$

$$\Pi_n = X^{-1}(\Delta_n) = \{p | p \in R^k, Xp \in \Delta_n\}$$

$$\Pi_\omega = X^{-1}(\Delta_\omega) = \{p | p \in R^k, Xp \in \Delta_\omega\} \qquad (24)$$

Let r_0, r_n, and r_ω denote the Euclidean distance measures between p_0 and Π_0, Π_n, and Π_ω, respectively. Let $\delta \in \Delta_0$, $t \in \Pi_0$, and $w_1 = [0, \ldots, 0, 1]$. Then

$$w_1 \delta = \delta_0 = 0 = w_1 Xp = w_1 Xt \qquad (25)$$

Denote the last row of X as X_l. Equation (25) states that $X_l t = 0$, which says that the parameter vectors contained in Π_0 are perpendicular to the last row of X. The shortest distance to Π_0 must lie along this direction and is given by

$$p_0 - t^* = \gamma X_l^T \qquad (26)$$

where γ is a constant and t^* is the closest vector to p_0. To compute γ, premultiply Eq. (26) by X_l. Thus,

$$X_l p_0 - X_l t^* = \gamma X_l X_l^T \qquad (27)$$

so that

$$\gamma = X_l p_0 / X_l X_l^T \qquad (28)$$

Substituting this into Eq. (26) yields

$$r_0 = p_0 X_l X_l^T p_0 / X_l X_l^T \qquad (29)$$

Using similar manipulations, the distance r_n is given by

$$r_n = p_0 X_f X_f^T p_0 / X_f X_f^T$$

where X_f is the first row of X. The remaining distance measure r_ω is computed by sweeping ω from zero to a sufficiently large value and using the minimum r over this range of ω. For a CLCV in Π_ω, δ is given by
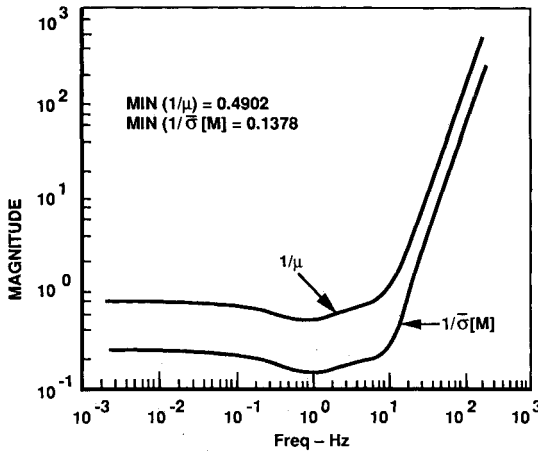
$$\delta = \Phi(\omega)\xi \qquad (30)$$
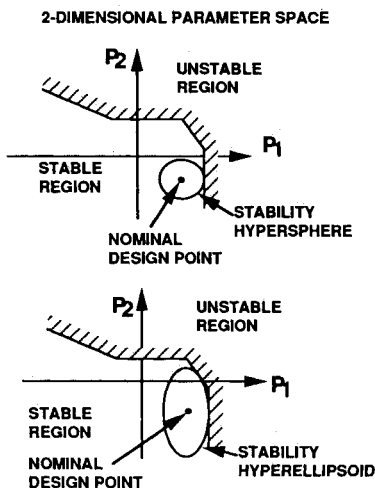
where ξ is of dimension $(n - 1) \times 1$ and is arbitrary. The $(n + 1) \times (n - 1)$ matrix $\Phi(\omega)$ is given by

$$\Phi(\omega) = \begin{bmatrix} 1 & & \\ 0 & & \\ \omega^2 & \ddots & 1 \\ & & 0 \\ & & \omega^2 \end{bmatrix} \qquad (31)$$

This matrix takes the $(n - 1)$-dimensional Hurwitz ξ polynomial (written as a vector) and multiplies into it two zeros at $\pm j\omega$. If $t_\omega \in \Pi_\omega$, then δ has two zeros on the $j\omega$ axis. Then,

$$Xt_\omega = \Phi(\omega)\xi \qquad (32)$$

Partition X and t_ω as follows:

$$X = [X_I X_J] \qquad (33)$$

$$t_\omega = \begin{bmatrix} t_I \\ t_J \end{bmatrix} \qquad (34)$$

where X_I is nonsingular. From Eq. (32)

$$X_I t_I = \Phi(\omega)\xi - X_J t_J \qquad (35)$$

Premultiply by the inverse of X_I

$$t_I = X_I^{-1}\Phi(\omega)\xi - X_I^{-1}X_J t_J \qquad (36)$$

Then, every $t_\omega \in \Pi_\omega$ is given by

$$t_\omega = \underbrace{\begin{bmatrix} X_I^{-1}\Phi(\omega) & X_I^{-1}X_J \\ 0 & I \end{bmatrix}}_{P(\omega)} \underbrace{\begin{bmatrix} \xi \\ t_J \end{bmatrix}}_{\xi_t} \qquad (37)$$

where $P(\omega)$ is a constant real matrix for each ω and ξ_t is an arbitrary real vector. If we sweep ξ_t over all real vectors, then Eq. (37) will yield all $t_\omega \in \Pi_\omega$. The distance measure $r(\omega)$ is the distance from t_ω to p_0, that is,

$$t_\omega - p_0 = P(\omega)\xi_t - p_0 \qquad (38)$$

with $r(\omega) = \|t_\omega - p_0\|^2$. To find the ξ_t that minimizes this distance (the closest to p_0), for a fixed ω, we compute the gradient with respect to ξ_t and equate to zero. Doing so yields

$$r^2(\omega) = p_0\{I - P^T(\omega)[(P(\omega)P(\omega)]^{-1}P^T(\omega)\}p_0 \qquad (39)$$

with

$$r_\omega = \inf_\omega r(\omega) \qquad (40)$$

Since all of the parameters in Eq. (39) are known, $r(\omega)$ is computed vs frequency, and the minimum value over ω is computed. The stability hypersphere radius $\rho(p_0) = \min(r_0, r_n, r_\omega)$.

A right matrix fraction description (MDF) $G(s) = N(s)d^{-1}(s)$ of the missile dynamics, Eq. (5), is given by

$$N(s) = \begin{bmatrix} 0 \\ 0 \end{bmatrix}s^4 + \begin{bmatrix} 0 \\ 0 \end{bmatrix}s^3 + \begin{bmatrix} \omega^2 V Z_\delta \\ 0 \end{bmatrix}s^2 + \begin{bmatrix} 0 \\ \omega^2 M_\delta \end{bmatrix}s^1$$

$$+ \begin{bmatrix} \omega^2 V(Z_\alpha M_\delta - Z_\delta M_\alpha) \\ \omega^2(Z_\delta M_\alpha - Z_\alpha M_\delta) \end{bmatrix}s^0$$

$$N(s) = n_4 s^4 + n_3 s^3 + n_2 s^2 + n_1 s + n_0 \qquad (41)$$

$$d(s) = s^4 + (2\zeta\omega - Z_\alpha)s^3 + (\omega^2 - M_\alpha - 2\zeta\omega Z_\alpha)s^2$$

$$- (2\zeta\omega M_\alpha + \omega^2 Z_\alpha)s - \omega^2 M_\alpha$$

$$= d_4 s^4 + d_3 s^3 + d_2 s^2 + d_1 s + d_0 \qquad (42)$$

The stability hypersphere tests determine bounds on the polynomial coefficients in this MFD. The left MFD for the controller $K(s) = d_c^{-1}(s)N_c^T(s)$ is

$$N_c^T(s) = [K_a K_q 0]s^2 + [K_a K_q(a_z + a_q)K_q]s^1$$

$$+ [K_a K_q a_z a_q K_q a_q]s^0$$

$$= n_{c2}s^2 + n_{c1}s + n_{c0} \qquad (43)$$

$$d_c(s) = s^2 + 0 \cdot s^1 + 0 \cdot s^0$$

$$= d_{c2}s^2 + d_{c1}s + d_{c0}$$

The controller coefficients are treated as known parameters. The CLCP $\delta(s)$ is

$$\delta(s) = \delta_6 s^6 + \cdots + \delta_1 s + \delta_0 \qquad (44)$$

The CLCV δ containing the polynomial coefficients is of dimension 7×1. Removing zero elements from the MDF of the missile dynamics (removing zero polynomial coefficients from the mapping), the following mapping is defined

$$\begin{bmatrix} & & & dc2 & \\ & & dc2 & dc1 & \\ & & dc2 & dc1 & dc0 \\ & & dc2 & dc1 & dc0 \\ nc12 & nc22 & dc2 & dc1 & dc0 \\ nc11 & nc21 & dc1 & dc0 \\ nc10 & nc20 & dc0 \end{bmatrix} \underbrace{}_{X_I} \begin{bmatrix} & & \\ & & \\ & nc12 & \\ nc22 & nc11 & \\ nc21 & nc10 \\ nc20 \end{bmatrix} \underbrace{}_{X_J} \begin{bmatrix} n01 \\ n02 \\ d0 \\ d1 \\ d2 \\ d3 \\ d4 \\ n12 \\ n21 \end{bmatrix}_{p} = \delta \qquad (45)$$

Substituting numerical values into p_0, Eq. (45) results in the nominal parameter vector are listed in Table 1. The stability hypersphere radius $\rho(p_0)$ is computed by evaluating the distance measures (r_0, r_n, r_ω). Details of this computation can be found in Bhattacharyya[5] or Wise.[6] Figure 5 displays the r_ω computation vs frequency. The stability hypersphere radius is $\rho(p_0) = \min (1.6 \times 10^9, 1.0, 18.4)$. This shows that the leading coefficient δ_n is the critical parameter. Table 1 shows the allowable parameter variation bounds determined by evenly distributing the stability hypersphere radius among the nine parameters in p.

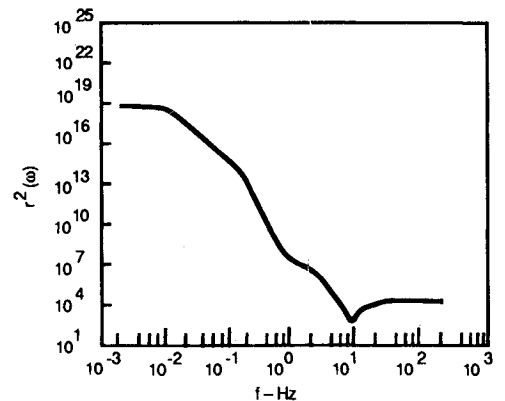This robustness prediction, when applied to each polynomial coefficient, results in a conservative allowable varia-

Fig. 5 Stability hypersphere radius—linear mapping.

Table 1 Stability hypersphere parameter variation bounds

Stability hypersphere radius $\rho(p_0)$ = 1.0	
Nominal value	Allowable variation
1.6644×10^9	$2.0276 \times 10^{-8}\%$
-1.8769×10^6	$1.7760 \times 10^{-5}\%$
-6.0922×10^5	$5.4715 \times 10^{-5}\%$
9.1110×10^3	$3.6583 \times 10^{-3}\%$
1.2928×10^4	$2.5784 \times 10^{-3}\%$
1.5950×10^2	$2.0899 \times 10^{-1}\%$
1.0	33.33%
-1.3386×10^6	$2.4902 \times 10^{-5}\%$
-2.4259×10^6	$1.3741 \times 10^{-5}\%$

tion. Several of the polynomial coefficients modeled in p did not vary with the uncertain aerodynamic stability derivatives. Also, several of the polynomial coefficients had large magnitudes. This translated into a very small allowable percentage variation.

This problem can be corrected by modeling the parameter vector p through the affine relationship $p = Ay + b$. The vector y contains only those parameters that are uncertain. The constant parameters that do not vary are incorporated into the vector b. Now, the CLCV δ is given by

$$Xp = XAy + Xb = \delta \qquad (46)$$

The parameter mapping obtained is as follows:

$$
\begin{bmatrix} n01 \\ d0 \\ n12 \\ d3 \\ n21 \\ n02 \\ d4 \\ d2 \\ d1 \end{bmatrix}
=
\begin{bmatrix}
\omega^2 V & 0 & 0 & 0 & 0 \\
0 & -\omega^2 & 0 & 0 & 0 \\
0 & 0 & -\omega^2 & 0 & 0 \\
0 & 0 & 0 & -1 & 0 \\
0 & 0 & 0 & 0 & \omega^2 V \\
\omega^2 & 0 & 0 & 0 & 0 \\
0 & 0 & 0 & 0 & 0 \\
0 & -1 & 0 & -2\zeta\omega & 0 \\
0 & -2\zeta\omega & 0 & -\omega^2 & 0
\end{bmatrix}
$$

$$
\times
\begin{bmatrix} Z_\alpha M_\delta - Z_\delta M_\alpha \\ M_\alpha \\ M_\delta \\ Z_\alpha \\ Z_\delta \end{bmatrix}
+
\begin{bmatrix} 0 \\ 0 \\ 0 \\ 2\zeta\omega \\ 0 \\ 0 \\ 1 \\ \omega^2 \\ 0 \end{bmatrix}
\qquad (47)
$$

The rows of the X matrix are reordered to match the parameter vector in Eq. (47). The goal is to compute the stability hypersphere radius in the parameter space of y. By introducing scaling, we can nondimensionalize the parameters in y and compute the stability hyperellipsoid, which will give better bounds on the individual parameter variations. Let $y = Qz$, where z is a vector of ones and Q contains the inverses of each of the parameters in y. This mapping maps all of the hyperspheres in the z parameter space into hyperellipsoids in the y parameter space. Thus,

$$p = AQz + b \qquad (48)$$

Performing the necessary calculations (see Wise[6]), the stability hypersphere radius is $\rho(p_0) = \min(1.0, \infty, 1.04)$. Evenly distributing this among the five parameters results in

$$\% \text{ bound on } \Delta p_i = \frac{\rho(p_0) \times 100\%}{\sqrt{5}} = 44.7\%$$

The parameter variation bounds using the affine parameter mapping combined with the hyperellipsoid scaling are greatly improved over the previous linear mapping. Conservatism will be present in the above bounds because the first parameter is a nonlinear combination of the four aerostability derivatives. If each parameter is allowed to vary by $\varepsilon = x\%/100$, the nonlinear parameter reduces the 44.7% variation bound to that of only 20.3%.

Lyapunov-Based Approach

The third stability hypersphere robustness test computes the magnitude bound on Δp using Lyapunov stability theory. Two models may be used in describing how the parameter uncertainties enter the closed-loop system matrix. The first, as in the previous polynomial case, models the parameter vector as $p = p_0 + \Delta p$, where p_0 is the nominal parameter vector and Δp the variation. With this model, Δp has the same units as p. This model is referred to as the unscaled model. The second model uses a multiplicative uncertainty model $p = p_0(1 + \Delta p)$, where the vector of variations Δp is dimensionless and each element is bounded by unity. This model is referred to as the scaled model. Since the stability hypersphere radius bounds the two norm of Δp, the units on the individual elements of Δp influence the degree of conservatism of the bound. Results for both of these parameter models are presented. This robustness test is applied to the earlier state-space model. The closed-loop model is

$$\dot{x} = (A_0 + \sum_{i=1}^{n} E_i \delta_i)x = A_{cl}x \qquad (49)$$

Since the nominal closed-loop linear time-invariant system is stable, we have, for positive definite Q,

$$A_0^T P + PA_0 + Q = 0 \qquad (50)$$

where P exists uniquely and is positive definite symmetric. Form the Lyapunov function $V(x) = x^T P x$. Using this $V(x)$, the closed-loop uncertain system, Eq. (49), will be stable if $V(x) > 0 \ \forall \ x$ and $\dot{V}(x) < 0 \ \forall \ x$. The first condition is satisfied for $V(x)$ since P is the positive definite solution of Eq. (50). The second condition is used to form an upper bound on the δ_i. To do this, we must determine how large δ_i can be such that $\dot{V}(x) \leq 0$. The derivative of $V(x)$ is given by

$$\dot{V}(x) = \dot{x}^T P x + x^T P \dot{x} \qquad (51)$$

Substituting for $\dot{x}$ yields

$$\dot{V}(x) = x^T \underbrace{(A_0^T P + PA_0)}_{-Q}x + x^T \left[\sum_{i=1}^{n} (E_i^T P + PE_i)\delta_i \right]x \qquad (52)$$

Using two-norm manipulations, the following inequality can be established (Bhattacharyya[5] or Wise[6]):

$$\|x\|_2^2 \left[\sum_{i=1}^{n} |\delta_i|(\|E_i^T P + PE_i\|_2) \right] \leq \underline{\sigma}[Q]x^T x \qquad (53)$$

Using Eq. (53), bounds on $|\delta_i|$ can be obtained by solving Eq. (50) for P. Equation (50) requires the Q matrix as an input. The square root of the sum of the $|\delta_i|$ in Eq. (53) forms the stability hypersphere radius. The choice of the Q matrix in Eq. (50) changes the stability hypersphere radius. This dependency forms an optimization problem in which the Q matrix is optimized to give the largest stability hypersphere radius.

The function to be maximized is

$$\rho^2(p_0, Q) = \frac{\underline{\sigma}^2[Q]}{\sum_{i=1}^{n} \|(E_i^T P + PE_i)\|_2^2} \qquad (54)$$

Unfortunately, little is known about the geometry of $\rho(p_0, Q)$. If $\rho(p_0, Q)$ were convex, then there would be an unique solution to Eq. (54) (our results show that it is not). To solve Eq. (54), a conjugate gradient optimization algorithm was used. The optimization was performed over the square root of Q ($Q = L^T L$) to preserve the positive definite property of the Q matrix.

The stability hypersphere radius results, using the Lyapunov optimization are shown in Table 2. These small bounds indicate extreme conservatism in the computation of the stability hypersphere radius. This conservatism results from the two-norm manipulations used to separate out the uncertainty parameter magnitudes [$|\delta_i|$ in Eq. (53)].

Kharitonov's Theorem

Kharitonov's theorem determines stability robustness by examining the Hurwitz properties of the characteristic polynomial. The version of Kharitonov's theorem presented here was taken from Argoun.[9]

The closed-loop characteristic polynomial $P_0(s)$ is given by

$$P_0(s) = d_c(s)d(s) + N_c^T(s)N(s)$$

$$= a_n s^n + \cdots + a_1 s + a_o \qquad (55)$$

where d_c, d, N_c, and N are defined in Eqs. (41–43). The coefficients in this polynomial have perturbations δa_i, where $|\delta a_i| < \Delta a_i$. The upper bound on Δa_i is determined when $P_0(s)$ is no longer Hurwitz. Using $s = j\omega$, $P_0(\omega)$ is factored into $P_0(\omega) = R_0(\omega) + j\omega Q_0(\omega)$ where

$$R_0(\omega) = a_0 - a_2\omega^2 + \cdots + (-1)^m + 2a_m\omega^m$$

$$Q_0(\omega) = a_1 - a_3\omega^2 + \cdots + (-1)^{(k-1)/2}a_k\omega^{k-1} \qquad (56)$$

n even: $m = n, k = n - 1$

n odd: $k = n, m = n - 1$

The perturbed polynomials are $R(\omega) = R_0(\omega) + \Delta R(\omega)$ and $Q(\omega) = Q_0(\omega) + \Delta Q(\omega)$, where ΔR and ΔQ model the extreme variations in the polynomial parameters. The stability robustness is determined by examining the Hurwitz properties of the following four polynomials:

$$R_1(\omega) = R_0(\omega) + \Delta R(\omega)$$

$$R_2(\omega) = R_0(\omega) - \Delta R(\omega)$$

$$Q_1(\omega) = Q_0(\omega) + \Delta Q(\omega) \qquad (57)$$

$$Q_2(\omega) = Q_0(\omega) - \Delta Q(\omega)$$

$$\Delta R(\omega) = \Delta a_0 + \Delta a_2\omega^2 + \cdots + \Delta a_m\omega^m$$

$$\Delta Q(\omega) = \Delta a_1 + \Delta a_3\omega^2 + \cdots + \Delta a_k\omega^{k-1}$$

The solution to $R_1(\omega) = 0$ and $R_2(\omega) = 0$ represents intersection frequencies of the extreme perturbed polynomials with the $j\omega$ axis. By ordering the roots in ascending order, we form frequency bands $\Delta_{\omega ri}$, $i = 1, \ldots, m/2$. Similarly, frequency bands $\Delta_{\omega qj}$, $j = 1, \ldots, k - 1/2$ are formed from $Q_1(\omega)$ and $Q_2(\omega)$. The perturbed polynomial $P(s)$ will be Hurwitz for all coefficient perturbations if $\Delta_{\omega r}$ and $\Delta_{\omega q}$ do not overlap.

Table 2 Lyapunov Optimization Results

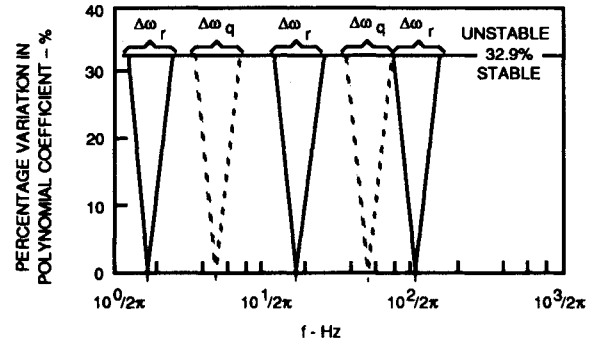| Parameter variation model	Stability hypersphere radius $\rho(p_0, Q)$	Allowable variation, %
$p = p_0 + \Delta p$	1.6208×10^{-4}	0.007
$p = p_0(1 + \Delta p)$	4.5107×10^{-4}	0.02

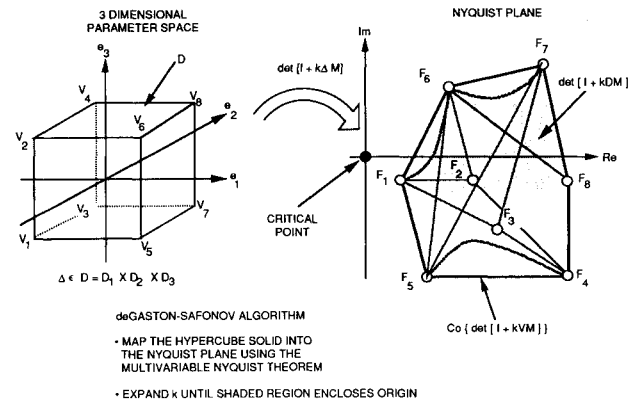Fig. 6 Robustness test results using Kharitonov's theorem.

Fig. 7 Real multiloop stability margin using the deGaston-Safonov algorithm.

Our results using this method are displayed in Fig. 6. The frequency intervals are shown to overlap at a 32.9% coefficient variation, and the frequency at which this occurs is 74.6 rad/s. This 32.9% variation bound describes the allowable variation on the polynomial coefficients of the closed-loop characteristic polynomial.

The aerodynamic stability derivatives enter the characteristic polynomial using the same parameter model as the stability hypersphere affine parameter mapping procedure. This creates one parameter that is a nonlinear combination of the four uncertain aerodynamic parameters. Since the nonlinear parameter must also satisfy the 32.9% allowable variation, the percentage variation on the independent aerodynamic stability derivatives is reduced to 15.3%.

This robustness test predicted the critical robustness frequency to be at 74.6 rad/s. This differs from the SSV μ robustness test, which identified 0.55 Hz (3.45 rad/s) as the critical frequency. Both the parameter variation bounds and critical frequencies differed between these two tests. This difference indicates a conservatism in this test that can be attributed to the parameter vector z model, Eq. (48), used to describe how the parameter variations enter the closed-loop polynomial.

Real Multiloop Stability Margin

At a fixed frequency ω, the deGaston-Safonov[10] real multiloop stability margin algorithm maps the space of uncertain parameters into the Nyquist plane using the multivariable Nyquist theorem. This procedure is shown in Fig. 7 for a three-dimensional parameter space. The solid cube in the parameter space represents all allowable combinations of uncertain parameters. The vertices of this cube are the extreme variations allowed for each parameter. The uncertain parameters and nominal system dynamics are modeled using the $M\Delta$ representation shown in Fig. 2. Each diagonal element of Δ describes an uncertain parameter. If there is a combi-

nation of parameters Δ_o in the parameter space that destabilizes the system, then the $\det[I + M\Delta_o] = 0$. This is a statement of the multivariable Nyquist theorem.

The bounds on the allowable parameter variations will form an n-dimensional polytope in the parameter space (in two dimensions, this is a rectangle). By scaling the parameter space, the polytope is transformed into a hypercube (a square in two dimensions). The scaled parameter-space hypercube solid, shown in Fig. 7, maps into the shaded region in the Nyquist plane using the $\det[I + kM\Delta]$ function. The scalar multiloop stability margin k multiplies Δ, and is expanded until the shaded region encloses the origin (the nominal design matrix M is stable so $k = 0$ is a stable point). When mapping the hypercube solid into the Nyquist plane, it is not computationally feasible to compute the shaded region in Fig. 7. However, the convex hull enclosing this region is easily computed.[15] The convex hull enclosing this region is formed by mapping the hypercube vertices V_i into the points F_i in the Nyquist plane. The outer boundary enclosing all vertex points F_i is then the convex hull co$\{\det[I + kVM]\}$. The multiloop stability margin k is then expanded until the origin is contained in the co$\{\det[I + kVM]\}$. This provides a lower bound on k, denoted k_l. A upper bound, denoted k_u, is formed by splitting the parameter space into subdomains and recomputing k for each subdomain. This procedure is then repeated, improving the accuracy of k. As the parameter space is split into smaller and smaller subdomains, the unstable region in the parameter space is determined. (The general idea is that the union of infinitesimal slices in the parameter space, mapped into the Nyquist plane, approaches the true image of the hypercube.) The stability margin k must be computed at each frequency along the $j\omega$ axis. The minimum k, vs frequency, is then used as the multiloop stability margin.

The minimum of the $1/\mu$ frequency response occurs at 0.55 Hz. Our results have identified this as the critical robustness frequency. (Our results using the multiloop stability margin have shown that larger parameter variation bounds are obtained at all other frequencies.) Since the SSV μ-test is conservative in its robustness prediction, the minimum of $1/\mu$ is used as the initial value for the multiloop stability margin: $k = \min 1/\mu$.

Using this value of k, the hypercube vertices are mapped into the Nyquist plane. This mapping is shown in Fig. 8. The convex hull co$\{\det[I + kVM]\}$ is constructed about the mapped vertex points. The co$\{\det[I + kVM]\}$ with $k = 0.4902$ does not intercept the origin. This indicates that $k_m > 0.4902$ and that the SSV μ-test is in fact conservative. Figure 8 also shows the co$\{\det[I + kVM]\}$ expanded in order to intercept the origin. This occurred at $k = 0.6044$. Thus, $k_l = 0.6044$. The vertex points on the co$\{\det[I + kVM]\}$ are labeled in order to determine which vertices are critical vertices. The vertices and mapped values at $k = 0.6044$ are listed in Table 3.
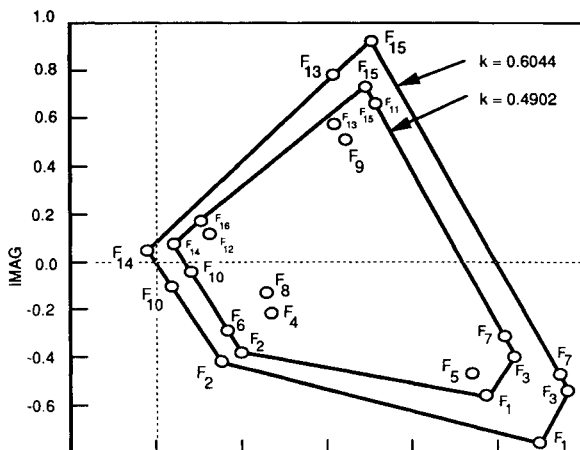

Fig. 8 Convex hull co[det(I + kVM)].

Table 3 Vertex mapping into Nyquist plane

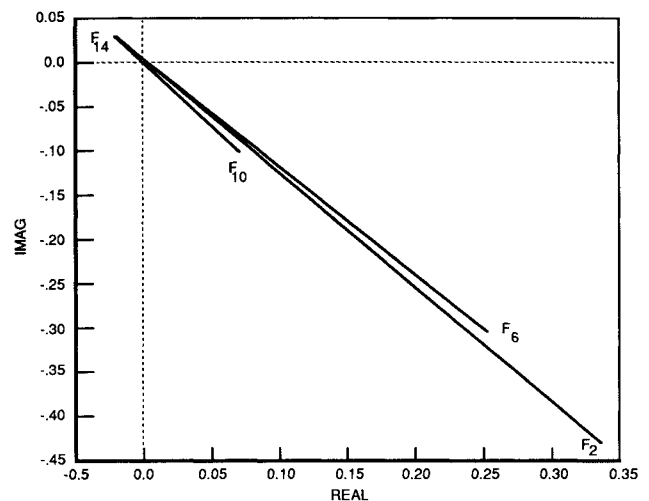| Vertex | | | | $\omega = 3.4387$ (rad/s) $k = 0.60446$ | |
				Re(Fi)	Imag(Fi)
V_1	-1	-1	-1	-1	2.325	-0.742
V_2	-1	-1	-1	1	2.222	-0.625
V_3	-1	-1	1	-1	2.450	-0.493
V_4	-1	-1	1	1	2.419	-0.455
V_5	-1	1	-1	-1	1.048	0.652
V_6	-1	1	-1	1	0.945	0.769
V_7	-1	1	1	-1	1.172	0.901
V_8	-1	1	1	1	1.142	0.939
V_9	1	-1	-1	-1	0.408	-0.446
V_{10}	1	-1	-1	1	0.305	-0.328
V_{11}	1	-1	1	-1	0.533	-0.196
V_{12}	1	-1	1	1	0.502	-0.158
V_{13}	1	-1	-1	-1	0.104	-0.118
V_{14}	1	1	-1	1	-0.102E-5	-0.354E-5
V_{15}	1	1	1	-1	0.228	0.132
V_{16}	1	1	1	1	0.197	0.169

Fig. 9 Rays from critical vertex F_{14}.

The next step in computing k_m is to determine the upper bound k_u. This is computed by examining the vertex paths between critical vertices. Figure 8 shows that the line segment from F_{14}-F_{10}-F_2 intercepts the origin. It is clear from Fig. 8 that vertex V_{14} is an isolated critical vertex. Figure 9 expands upon this critical area in the Nyquist plane. Rays are drawn from F_{14} to the mapped vertex points F_2, F_6, and F_{10}. Figure 9 clearly shows that the convex hull is made up of line segments from F_{14} to F_{10} and F_{10} to F_2. This indicates that V_{14} and V_{10} are two isolated critical vertices.

The isolated critical vertices V_{10} and V_{14} are

$$V_{10} \quad 1.0 \quad -1.0 \quad -1.0 \quad 1.0$$
$$V_{14} \quad 1.0 \quad 1.0 \quad -1.0 \quad 1.0$$

These two vertices differ only in the second coordinate. A mapping theorem taken from Zadeh and Desoer[13] states that any path along a single coordinate in the parameter space maps into a straight line in the Nyquist plane. This guarantees that any point on the face of the hypercube mapped into the Nyquist plane will be contained in the convex hull formed by the mapped vertices. This is true only for real parameter variations. (If the parameters under variation were complex, any path along a single coordinate would trace an arc in the Nyquist plane. Thus, points contained on the face of a complex parameter hypercube mapped into the Nyquist plane need not be contained in the convex hull formed by the hypercube vertices. This fact precludes the use of parameter space methods in analyzing complex parameter variations.)

The line segment connecting the critical vertices V_{10} and V_{14} is contained in the mapped hypercube image $\det[I + kDM]$. The value $k = 0.6044$ is the multiloop stability margin k_m. Applying this uniformly over each of the aeroparameters produces a 61% variation bound.

The two critical hypercube vertices identified by the multiloop stability margin differed in the second coordinate of $[Z_\alpha \ Z_\delta \ M_\alpha \ M_\delta]$. Interpolating to the origin between these two vertices yields $\Delta_o = (0.6044)\text{diag}[1.\ 0.99\ -1.\ 1.]$ as the destabilizing parameter variation. The parameters Z_α, M_α, and M_δ all must be at the extreme variation of 61% for the system to be unstable.

Monte Carlo Eigenanalysis

Parameter variation bounds were also determined using a Monte Carlo eigenanalysis. We examined the eigenvalues of the closed-loop system, Eq. (5), randomly perturbing the aerodynamic stability derivatives. Each aeroparameter was varied by the same percentage. We examined 2000 closed-loop system matrices at each percentage variation level. At a 60% variation level, the closed-loop system was always found to be stable. At a 61% variation level, several unstable closed-loop systems were formed. We saved the aeroparameter combinations that caused instability for comparison with our other robustness test predictions. The aeroparameter combinations that caused instability identically matched the region in the parameter space predicted by the real multiloop stability margin algorithm.

The Monte Carlo approach used here randomly perturbed the aerodynamic stability derivatives using a fixed, bounded, percentage variation. This approach results in parameter combinations that fill the volume of a hypercube in the parameter space (since they are uniformly distributed over an interval), rather than perturbing the parameters over the face of the hypercube. In comparison with the other robustness tests, no additional information, such as the critical robustness frequency, is obtained from our Monte Carlo approach.

Robustness Test Summary

Figure 10 summarizes the stability robustness predictions obtained from each robustness test and the Monte Carlo eigenanalysis. The only robustness test not found to be conservative was the real multiloop stability margin calculation by deGaston and Safonov.

Conclusions

Of the polynomial-based robustness tests, we found the stability hypersphere radius calculation using the affine parameter mapping to be the least conservative. For problems where the polynomial coefficients are linear in the uncertain parameters, this robustness test produces nonconservative results. The stability hypersphere radius calculation using the state-space model (Lyapunov approach) proved too conservative to be useful. The two-norm manipulations used to separate out the parameter uncertainties (similar to the triangle inequality) introduce too much conservatism for this approach to be a useful robustness test. The SSV μ-test produced very reasonable results. The software and models used in the SSV μ-test make this test a very powerful analysis tool. However, our experience using the SSV μ-test for problems with large numbers of scalar real parameter uncertainties (nine) indicate added conservatism, as compared to the results presented here. The real stability margin algorithm of deGaston and Safonov produced the best results. However, it is the most complicated approach examined.

The computational requirements greatly differ between these robustness tests. The uncertainty bounds from the small gain theorem, stability hypersphere-polynomial test, and Kharitonov's theorem were the easiest to compute and posed no computational difficulties. The stability hypersphere-Lyapunov test required a conjugate gradient optimization, in which commercial software is readily available. Similarly, the SSV μ-test can also be computed using commercial software. The real margin algorithm was by far the most difficult approach to implement and suffers from an exponential explosion in the number of hypercube vertex points that have to be analyzed. However, reasonable cpu times using our software[15] have been obtained analyzing problems with as many as nine parameters.

Several of the robustness tests presented here provide additional information, such as critical robustness frequency, in addition to computing bounds on the allowable parameter variations. The SSV μ and the real multiloop stability margin predicted the same critical robustness frequency.

Future research in developing robustness tests should focus on reducing the conservatism in the parameter variation bounds and in reducing the computational requirements. Also, research in developing nonconservative robustness tests for simultaneous real and complex uncertainties would greatly benefit the industry.

References

[1] Doyle, J. C., "Analysis of Feedback Systems With Structured Uncertainties," *IEE Proceedings*, Vol. 129, No. 6, 1982, pp. 260–265.

[2] Doyle, J. C., Wall, J. E., and Stein, G., "Performance and Robustness Analysis for Structured Uncertainty," *Proceedings of the 22nd IEEE Conference on Decision and Control*, IEEE, New York, 1982, pp. 629–636.

[3] Wise, K. A., "Singular Value Robustness Tests for Missile Autopilot Uncertainties," *Journal of Guidance, Control, and Dynamics*, Vol. 14, No. 3, 1991, pp. 597–606.

[4] Biernacki, R. M., Hwang, H., and Bhattacharyya, S. P., "Robust Stability With Structured Real Parameter Perturbations," *IEEE Transactions on Automatic Control*, Vol. AC-32, No. 6, 1987, pp. 495–506.

[5] Bhattacharyya, S. P., *Robust Stabilization Against Structured Perturbations*, Springer-Verlag, New York, 1987.

[6] Wise, K. A., "Missile Autopilot Robustness To Uncertain Aerodynamics: Stability Hypersphere Radius Calculation," *Journal of Guidance, Control, and Dynamics*, Vol. 14, No. 1, 1991, pp. 166–175.

[7] Yeung, K. S., and Wang, S. S., "A Simple Proof of Kharitonov's Theorem," *IEEE Transactions on Automatic Control*, Vol. AC-32, No. 9, 1987, pp. 822–823.

[8] Barmish, B. R., and DeMarco, C. L., "Criteria for Robust Stability With Structured Uncertainty: A Perspective," *Proceedings of*

ROBUSTNESS THEORY	% PERTURBATION
SMALL GAIN THEOREM	13.8%
SSVμ (UNIT WEIGHTS)	49.0%
STABILITY HYPERSPHERE Xp = δ	0.1%
STABILITY HYPERSPHERE p = A α₀+b	20.3%
STABILITY HYPERSPHERE (LYAPUNOV - UNSCALED)	0.007%
STABILITY HYPERSPHERE (LYAPUNOV - SCALED)	0.02%
KHARITONOV'S THEOREM	15.3%
deGASTON-SAFONOV	60.44%
MONTE CARLO EIGEN ANALYSIS	60-61%

Fig. 10 Robustness test summary.

the American Control Conference, 1987, pp. 476–481.

[9]Argoun, M. B., "Frequency Domain Conditions for the Stability of Perturbed Polynomials," *IEEE Transactions on Automatic Control*, Vol. AC-32, No. 10 1987, pp. 913–916.

[10]deGaston, R. R., and Safonov, M. "Exact Calculation of the Multiloop Stability Margin," *IEEE Transactions on Automatic Control*, Vol. 33, No. 2, 1988, pp. 156–171.

[11]Sideris, A., and Pena, R., "Robustness Margin Calculation with Dynamic and Real Parametric Uncertainty," *Proceedings of the American Control Conference*, 1988, pp. 1201–1206.

[12]Wise, K. A., "Optimizing Singular Value Robustness Measures In A Conventional Bank-to-Turn Missile Autopilot Design," *Proceedings of the AIAA GNC Conference*, AIAA, Washington, DC, pp. 296–306; also AIAA Paper 88-4089, Aug. 1988.

[13]Zadeh, L. A., and Desoer, C. A., *Linear System Theory: The State Space Approach*, McGraw-Hill, New York, 1963.

[14]Morton, B. G., "New Applications of Mu to Real Parameter Variation Problems," *Proceedings of the 25th IEEE Conference on Decision and Control*, IEEE, New York, 1985.

[15]Wise, K. A., Mears, B. C., Tang, C., and Godwanhi, A., "A Convex Hull Program Evaluating Control System Robustness To Real Parameter Variations," *Proceedings of the AIAA Guidance, Navigation, and Control Conference*, AIAA, Washington, DC, 1990, pp. 223–231.

[16]Doyle, J. C., Balas, G., and Packard, A., "MUSYN Robust Control Short Course Lecture Notes," Arcadia, CA, Sept. 1989.